J Nanopart Res (2015) 17:143
DOI 10.1007/s11051-015-2950-4

RESEARCH PAPER

Synthesis, photophysical analysis, and in vitro cytotoxicity assessment of the multifunctional (magnetic and luminescent) core@shell nanomaterial based on lanthanide-doped orthovanadates

Agata Szczeszak · Anna Ekner-Grzyb · Marcin Runowski · Lucyna Mrówczyńska · Tomasz Grzyb · Stefan Lis

Received: 16 November 2014 / Accepted: 6 March 2015 / Published online: 17 March 2015

Abstract Rare earths orthovanadates ($REVO_4$) doped with luminescent lanthanide ions (Ln^{3+}) play an important role as promising light-emitting materials. Gadolinium orthovanadate exhibits strong absorption of ultraviolet radiation and as a matrix doped with Eu^{3+} ions is well known for its efficient and intense red emission, induced by energy transfer from the VO_4^{3-} groups to Eu^{3+} ions. In the presented study, Fe_3O_4@SiO_2@$GdVO_4$:Eu^{3+} 5 % nanomaterial was investigated. The core@shell structures demonstrate attractive properties, such as higher thermal stability, enhanced water solubility, increased optical response, higher luminescence, longer decay times, and magnetic properties. Silica coating may protect nanocrystals from the surrounding environment. Therefore, such silica-covered nanoparticles (NPs) are successfully utilized in biomedical research. Multifunctional magnetic nanophosphors are very interesting due to their potential biomedical applications such as magnetic resonance imaging, hyperthermic treatment, and drug delivery. Therefore, the aim of our study was to investigate photophysical, chemical, and biological properties of multifunctional $REVO_4$ doped with Ln^{3+}. Moreover, the studied NPs did not affect erythrocyte sedimentation rate, cell membrane permeability, and morphology of human red blood cells.

Keywords Nanoparticles · Multifunctional nanostructures · Surface decoration · Erythrocytes · Hemolysis · Human red blood cells · Health effects

A. Szczeszak · M. Runowski · T. Grzyb · S. Lis (✉)
Department of Rare Earths, Faculty of Chemistry, Adam Mickiewicz University, Grunwaldzka 6, 60-780 Poznań, Poland
e-mail: blis@amu.edu.pl

A. Ekner-Grzyb
Department of Behavioural Ecology, Faculty of Biology, Adam Mickiewicz University, Umultowska 89, 61-614 Poznań, Poland

L. Mrówczyńska
Department of Cell Biology, Faculty of Biology, Adam Mickiewicz University, Umultowska 89, 61-614 Poznań, Poland

Introduction

The rapid development of functional nanomaterials has been observed over the last few years (Xue et al. 2011; Liu et al. 2011; Limaye et al. 2011; Yoo and Lee 2014). Nanomaterials are composed of particles having at least one dimension in the range of 1–100 nm (Henglein 1987). Due to the small size, such nanoparticles have large surface area-to-volume ratio and a possibility of the formation of stable aqueous colloids. What is more, they are smaller than living cells, which facilitates their interactions with the desired organic structures, investigated in vitro and in vivo (Selvan et al. 2009). This is the crucial feature of nanomaterials allowing their applications in

biology and medicine, e.g., drug carriers, contrast agents, or biomarkers.

Lanthanide (Ln^{3+})-doped compounds are well known as efficient phosphors (light emitters), applied in optoelectronics, forensics, documents protection, new light sources, solar cells, etc. (Dosev et al. 2008; Chander 2005). They exhibit bright multicolor luminescence, long radiative lifetimes (in the range of ms), large Stokes shifts, narrow emission bands, and tunable luminescence dependent on the coordination environment (Dosev et al. 2008; Chander 2005; Grzyb et al. 2014, 2012a). Because of the intensive and bright luminescence, Eu^{3+} and Tb^{3+} ions are commonly used as red and green light sources, respectively. The direct excitation of Ln^{3+} ions is usually inefficient, because of the forbidden character of the 4f-4f transitions, in these ions. That is why, the energy transfer (ET) and charge transfer (CT) phenomena are often used to increase the luminescence efficiency of such compounds (Grzyb et al. 2014, 2012b). Ce^{3+} and Gd^{3+} ions are well-known energy donors (light harvesting ions) in the case of UV-light excitation (energy down-conversion) (Grzyb et al. 2012a; Yang et al. 2011), and Yb^{3+} ions are used as energy donors during IR-light excitation (energy up-conversion) (Niu et al. 2011).

Gadolinium orthovanadate ($GdVO_4$) exhibits many advantages, e.g., high thermal conductivity, broad emission, and large absorption cross section. Moreover, Gd^{3+} ($4f^7$, ^8S)-based matrices have played an important role as phosphors due to relatively high energy of the lowest excited state in connection with stability of a half-filled of the ground state of gadolinium (Wu and Yan 2008). $GdVO_4$ shows strong absorption of ultraviolet (UV) radiation, and doping with Eu^{3+} ions enables the efficient and intense red emission, induced by ET from the VO_4^{3-} groups to Eu^{3+} ions (Li et al. 2011).

The luminescent nanomaterials based on the lanthanide-doped nanoparticles have large interest in the case of scientific, industrial, and biological applications. In comparison to the organic dyes and semiconducting quantum dots, they have all of the mentioned advantages characteristic of Ln^{3+} ions and also reveal photo- and thermo-stability, resistance to oxidation, and low cytotoxicity (Blasse and Grabmaier 1994; Binnemans 2009; Grzyb et al. 2013; Runowski et al. 2013).

Core@shell-type nanostructures are composed of at least two distinguished phases of the core and the shell. The nanosized core as well as nanoshell can be inert or active, i.e., exhibits selective affinity to the desired structures, luminescence, magnetism, catalytic activity, etc. (Grzyb et al. 2013; Haidar 2010; Chen et al. 2011; Runowski et al. 2012). What is more, the shell can be appropriately modified according to the expected requirements of such composite materials (Runowski et al. 2013; Lu et al. 2010; Hu et al. 2010). The external shell may also function as a protective barrier from the destructive impact of the environment, e.g., high temperature, oxidizing atmosphere, aggressive agents, and so on (Park et al. 2010). Currently, the fabrication of bifunctional and multifunctional nanomaterials attracts much interest of scientists because of the benefits resulting from their multimodal nature (Chen et al. 2011; Runowski et al. 2012; Lou et al. 2011; Kang et al. 2013b; Zhou et al. 2014; Deshmukh et al. 2014).

The nanomaterials exhibiting simultaneously luminescence and magnetism have been intensively studied over the last few years (Runowski et al. 2012; Lou et al. 2011; Gai et al. 2010; Wang et al. 2014; Tong et al. 2013; Ma et al. 2014). Such nanostructures can be used in luminescent tracing combined with magnetic separation, multimodal bioimaging (simultaneous luminescence and magnetic imaging), novel targeted treatment such as hyperthermia combined with photodynamic therapy, or highly specific drug delivery (Selvan et al. 2009; Lou et al. 2011; Gai et al. 2010; Corr et al. 2008). Except of the mentioned bioapplications, such multifunctional luminescent-magnetic nanomaterials can be applied in localized (thanks to the luminescence) magnetic enrichment of the diluted precious substances and organic structures (Hu et al. 2010). They can be also used as novel, hard to imitate protection materials, due to their magnetic properties and possible luminescence coding (unique combination of the spectral lines in the emission spectra) (Hölsä 2009; Cheng et al. 2008).

Core@shell-type nanoparticles seem to function perfectly as the mentioned luminescent-magnetic materials. The external shell can protect the magnetic core from a negative impact of the environment as well as increase the selectivity and affinity of such nanosystem. Moreover, if the shell of the given nanomaterial is decorated with luminescent nanoparticles, the final nanomaterial becomes multifunctional, which creates many new possibilities of its application in medical, biological, scientific, and industrial areas.

Despite the importance of vanadates doped with lanthanide ions, only a few studies concerned their

utilization in biology and medical science (Cheng et al. 2012; Shanta Singh et al. 2013; Wang et al. 2009), whereas some of the research showed that Ln:$GdVO_4$ nanoparticles (NPs) may have potential application in optical or MRI images (Huang et al. 2013; Nuñez et al. 2013; Kang et al. 2013a; Yin et al. 2012). In addition, combination of magnetic and luminescent properties of nanoparticles makes them particularly useful. Such multifunctional nanomaterials allow the simultaneous imaging using MRI techniques and phosphorescence (multimodal imaging) (Zhou et al. 2014). However, the first step toward utilization of chemical compounds in biological research is to determine their biocompatibility (Gnach et al. 2014). Therefore, one of the aims of our study was to investigate the cytotoxic effect of studied NPs on human cells. One of the most convenient systems for the study of cytotoxic properties of new chemical compounds are erythrocytes. To the best of our knowledge, there is no study on the influence of multifunctional, luminescent-magnetic nanocrystals doped with lanthanide ions on red blood cells.

Here we report the synthesis and characterization of the multifunctional core@shell-type nanomaterial exhibiting simultaneously luminescent and magnetic properties—Fe_3O_4@SiO_2@$GdVO_4$:Eu^{3+} 5 %. Our intention was to obtain an efficient, reproducible, and non-cytotoxic luminescent-magnetic nanomaterial based on the commonly used chemical compound, which can be used in various bioapplications as well as in science and industry. The desired product should also exhibit relatively long radiative lifetime (in the range of ms), in order to eliminate the potential background radiation, in the case of its bioapplications. Because of the potential bioapplications, we examined its biological properties, namely the in vitro cytotoxicity assays on human erythrocytes. Magnetite nanoparticles, Fe_3O_4, were used as nanocores because they can be synthesized in a simple and inexpensive way as nanocrystalline magnetic particles. There are many reports on their application as magnetic cores in core@shell-type nanostructures as well (Runowski et al. 2012; Lu et al. 2010; Hu et al. 2010; Park et al. 2010). The as-prepared magnetic cores were coated with silica shell by simple hydrolysis and subsequent co-condensation of silane derivatives. Silica shell provides cores separation from the environment, prevents their agglomeration, and simplifies the surface modification of the nanostructures synthesized (Runowski et al. 2013; Hu et al. 2010). The formed silica nanoshell facilitated subsequent surface decoration with $GdVO_4$:Eu^{3+} 5 % nanoparticles, exhibiting intensive red emission.

Materials and methods

Synthesis of Fe_3O_4

The magnetite nanoparticles were synthesized by a modified Massart method (Massart 1981). The water used in the whole experiment was purged with nitrogen, in order to remove dissolved oxygen. 0.3475 g of $FeSO_4$*7-H_2O was dissolved in 5 mL of water with the addition of 0.05 mL of 30 % HCl (to suppress oxidation of Fe^{2+} ions) and mixed with 0.675 g of $FeCl_3$*$6H_2O$, previously dissolved in 20 mL of water. The as-prepared solution of iron species was added dropwise (in 3 min) to the diluted solution of ammonia (100 mL of water and 10 mL of concentrated ammonia), which was magnetically stirred. After this, the black precipitate of magnetite nanoparticles (Fe_3O_4) appeared immediately. In order to improve the crystallinity of the product, the whole system was heated up to 353 K, for 30 min, with continuous magnetic stirring, under a protective layer of gasoline. Afterward, the obtained product was extracted with 20 mL of 1 % oleic acid in cyclohexane solution (0.2 mL of oleic acid dissolved in 20 mL of cyclohexane).

Synthesis of Fe_3O_4@SiO_2

In order to get non-agglomerated and monodispersive core@shell nanoparticles, a reverse microemulsion method was used to prepare Fe_3O_4@SiO_2 core@shell NPs (Ding et al. 2012). 2 g of Igepal CO-520 (nonionic surfactant) was dispersed in 40 mL of cyclohexane and sonicated for 10 min. Then 3.2 mL of Fe_3O_4 nanoparticles from cyclohexane solution (40 mg, 12.5 mg/mL) was added to the above solution. Subsequently, 0.4 mL of ammonium hydroxide (25 %) was added to the above mixture and sonicated for 15 min to get clear and homogeneous solution. Finally, 0.1 mL of TEOS (tetraethoxysilane) was added. After 1 h 0.1 mL of TEOS and 0.1 mL of 45 % aqueous solution of EDATAS (N-(trimethoxysilylpropyl)ethylenediamine triacetic acid, trisodium salt—silane derivative of EDTA) were added. The role of EDATAS was to facilitate the homogeneous silica decoration with

luminescent nanoparticles, by the chelating properties of EDTA molecules toward Ln^{3+} ions (precipitation of lanthanide nanoparticles on the silica surface). The whole reaction lasted 24 h using magnetic stirrer. The resulting Fe_3O_4@SiO_2 core@shell NPs were collected by precipitation with acetone and ethanol. Afterward, the product was magnetically purified by washing several times with ethanol and water. The final product was redispersed in ethanol, forming ultra-stable colloidal solution.

Synthesis of Fe_3O_4/SiO_2@$GdVO_4$:Eu^{3+} 5 %

The synthesis was performed to get 2.2 mg of the final product, composed of 2 mg magnetic core (Fe_3O_4@-SiO_2) and 0.2 mg of the luminescent shell ($GdVO_4$:Eu^{3+} 5 %). The aqueous solutions of $Gd(NO_3)_3$ (55 μL 0.0127 M) and $Eu(NO_3)_3$ (32 μL 0.00114 M) were mixed together and vigorously stirred at ambient conditions. Afterward, 0.53 mL of the colloidal Fe_3O_4/SiO_2 (C = 3.8 mg/mL − 2 mg) was added to the previous solution. The as-prepared colloid was intensively shaken and stirred. When the colloidal solution became homogeneous, 1 mL of NH_4VO_3 aqueous solution (C = 0.086 mg/mL − stoichiometric amount) was slowly added, drop by drop. When the synthesis was completed (even before purification of the product), the formed composite nanomaterial exhibited an intensive red luminescence and a response for the applied magnetic field (NdFeB magnet). Here it is worth noting that after magnet capture, the solution was fully transparent and did not illuminate under UV light (only the solid phase attracted by the magnet exhibited luminescence). After that, the whole product was thoroughly purified by the magnet capture and washing several times with ethanol and water.

Cytotoxicity assay and erythrocytes shape under the test compounds

Erythrocyte preparation

Fresh human erythrocyte suspensions were obtained from the blood bank. The erythrocytes were washed three times (3000 rpm, 10 min) in phosphate-buffered saline (PBS, pH 7.4) supplemented with 10 mM glucose. After washing, cells were suspended in the buffer at 1.65×10^9 cells/mL, stored at 277 K and used within 5 h.

Erythrocyte sedimentation under nanomaterials treatment

Erythrocytes (1.65×10^8 cells/mL) were incubated with nanoparticles in Eppendorf vials for 60 min, at 310 K, under gently mixing. Three different concentrations (1, 0.1, 0.01 mg/mL) of the nanoparticles were investigated. The cells incubated only in PBS (pH 7.4), and supplemented with 10 mM glucose, were taken as a control series. The erythrocyte sedimentation rate (ESR) was recorded by the use of a digital camera after 1 h. The morphologies of both treated and control erythrocytes were estimated using a light microscope. The erythrocyte shape was classified according to Bessis (Bessis et al. 1973). After observation, erythrocytes were fixed in 0.1 % glutaraldehyde for 1 h, at room temperature (RT). Each sample was repeated three times, and the experiments were repeated three times with erythrocytes from different donors.

Hemolysis assays

Erythrocytes (1.65×10^8 cells/mL, ~1.5 hematocrit) were incubated in PBS (pH 7.4) supplemented with 10 mM glucose and containing test compounds for 60 min at 310 K in a shaking water bath. Three different concentrations (1, 0.1, 0.01 mg/mL) for all of the nanoparticles were investigated. Erythrocytes incubated only in PBS were taken as the control. Following the incubation, the erythrocyte suspensions were centrifuged (3000 rpm, 10 min), and the degree of hemolysis was estimated by monitoring the hemoglobin in the supernatant as previously reported (Jasiewicz et al. 2014). The results were expressed as a percentage (%) of hemolysis. Hemolysis 0 % was taken as the absorbance of the supernatant of the erythrocyte suspensions in PBS only, while the total hemolysis (100 %) was determined when PBS was replaced by distilled water. Each sample was repeated three times and the experiments were repeated three times with erythrocytes from different donors.

Scanning electron microscope studies of erythrocytes shape alterations

Erythrocytes were fixed in 0.1 % glutaraldehyde for 1 h at room temperature. The fixed cells were washed by exchanging of the supernatant with PBS. The

samples were gently vortexed and the cells were fixed with 2 % glutaraldehyde for another hour. After washing as above, the cells were post-fixed with 1 % OsO_4 for 30 min at RT. The supernatant was exchanged with PBS, and samples were gently vortexed. Fixed cells were dehydrated in a series of ethanol solutions (50, 60, 70, 80, 90, 95, and 100 %), gold sputtered, and examined using an *EVO 40* (ZEISS, Germany) scanning electron microscope.

Characterization

X-ray diffraction pattern (XRD) was recorded using a Bruker AXS D8 Advance diffractometer in the Bragg–Brentano geometry, with $CuK_{\alpha 1}$ radiation (1.5406 Å) in the 2θ ranges from 6 to 60°. The XRD pattern was assigned to the Joint Committee on Powder Diffraction Standards (JCPDS) database. The transmission electron microscopy (TEM) images were recorded at FEI Tecnai G2 20 X-TWIN transmission electron microscope, by an accelerating voltage of 200 kV. The SEM images were done using *EVO 40* (ZEISS, Germany) scanning electron microscope. The IR absorption spectrum was recorded between 400 and 4000 cm^{-1} on the FT-IR spectrophotometer, JASCO 4200. The material was mixed with KBr and then pressed to disks. Luminescence properties of the synthesized samples were collected for the aqueous colloidal solution with concentration of 1 mg of the core@shell per 1 mL of colloid at a Hitachi F-7000 Fluorescence Spectrophotometer at RT (300 and 77 K) with the 150 W xenon lamp as the excitation source. Excitation and emission spectra were corrected for the instrumental response.

Results and disscussion

The multifunctional core@shell-type nanostructure of Fe_3O_4@SiO_2@$GdVO_4$:Eu^{3+} 5 % was synthesized using in sequence modified Massart method, reverse microemulsion method, and precipitation reaction (Fig. 1). For the synthesis of core@shell nanostructures and their surface modification, we used the modified methods reported in our previous papers (Runowski et al. 2011, 2014). Its structure and morphology was determined using XRD pattern, TEM images, and IR spectra.

In Fig. 2, the XRD pattern of the obtained nanomaterial is presented. It is well seen that all the diffraction peaks are well consistent with the diffraction lines of the reference patterns of the cubic *Fd-3 m* Fe_3O_4 and tetragonal $I4_1/amd$ $GdVO_4$. The presence of SiO_2 is not visible due to its amorphous character. All of the reflexes are broadened, which is related to the small size of crystallites. Additional reflexes are not visible, which confirmed lack of contamination in the nanomaterial obtained.

In Fig. 3, the FT-IR spectra of the Fe_3O_4, Fe_3O_4@SiO_2 and Fe_3O_4@SiO_2@$GdVO_4$:Eu^{3+} 5 % nanocrystals are presented. All the spectra show the most intense and broad band at 3444 cm^{-1} related to O–H stretching vibrations of hydrogen-bonded H_2O molecules (adsorbed on the nanoparticles surface). Additionally, at about 1633 cm^{-1}, the absorption peak associated also with water molecules was observed (deformation vibrations of the O–H groups). In the spectrum of Fe_3O_4, the peaks in the range of 2800–3000 cm^{-1} are related to νC-H vibration, and come from cyclohexane and oleic acid molecules (used during extraction) adsorbed on the nanoparticles surface (as other no described peaks at lower wavenumbers). The spectra of the Fe_3O_4@SiO_2 and Fe_3O_4@SiO_2@$GdVO_4$:Eu^{3+} 5 % nanostructures exhibit four peaks characteristic of silica: νSi–O–Si(asym) (1092 cm^{-1}), νSi–O^-(957 cm^{-1}), νSi–O–Si(sym) (799 cm^{-1}), and σSi–O–Si (464 cm^{-1}). The absorption bands denoted at 636 cm^{-1} as νFe–O and at 801 cm^{-1} as νVO_4^{3-} vibrations were recorded, which confirmed the presence of magnetic core and luminescent shell in the nanomaterials obtained. The performed FT-IR measurements proved the formation of the core@shell-type nanomaterials.

The size and morphology of the Fe_3O_4@SiO_2@$GdVO_4$:Eu^{3+} 5 % nanocrystals were analyzed by TEM. As shown in Fig. 4, the nanoparticles exhibit spherical shape, and the crystallites are rather agglomerated. An average core@shell nanoparticles size is about 40 nm. TEM images showed clearly formation of the core@shell-type structures, and the presence of vanadate nanoparticles decorated on the silica surface. What is more, there was no observed bare silica (core-free silica) during the product analysis.

The bifunctional magnetic-luminescent core@shell exhibited strong visible red emission under UV excitation due to doping of the Eu^{3+} ions. In Fig. 5 (left) there is an excitation spectrum monitored for the

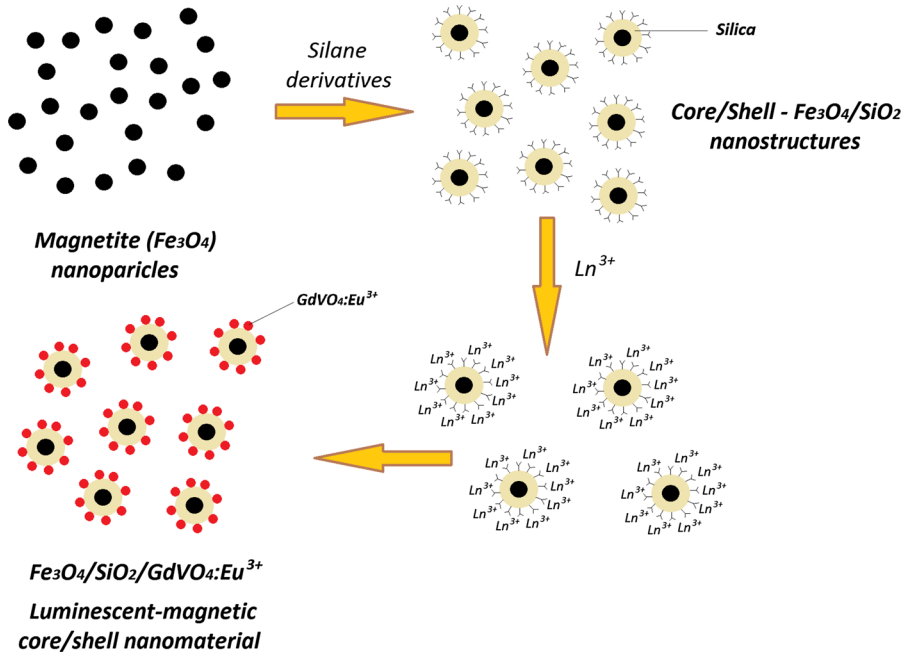

Fig. 1 Scheme of the synthesis of the Fe_3O_4@SiO_2@$GdVO_4$:Eu^{3+} 5 % nanostructures

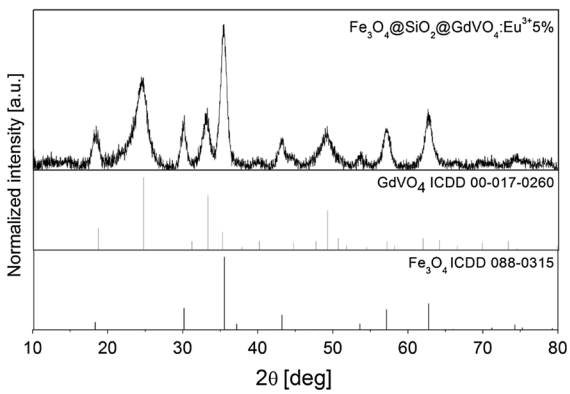

Fig. 2 XRD pattern of the synthesized Fe_3O_4 and Fe_3O_4@SiO_2@$GdVO_4$:Eu^{3+} 5 % nanocrystals

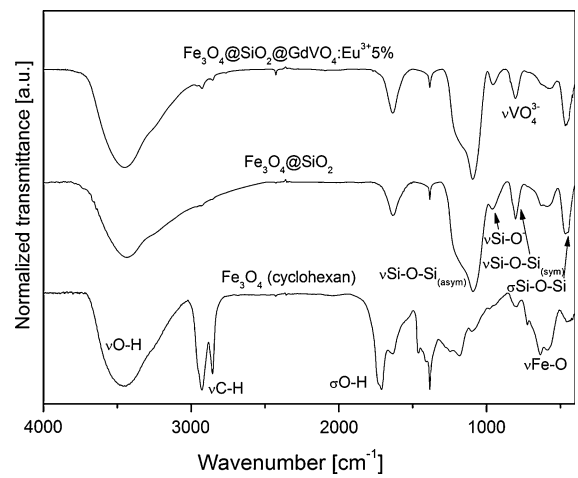

Fig. 3 IR spectra of the synthesized Fe_3O_4, Fe_3O_4@SiO_2 and Fe_3O_4@SiO_2@$GdVO_4$:Eu^{3+} 5 % nanomaterials

Eu^{3+} ions emission at 616 nm. The spectrum shows one intense and broad band peaking at $\lambda = 276$ nm, related to the CT bands $O^{2-} \rightarrow Eu^{3+}$. Figure 5 (right) presents the emission spectrum, which consists of five sharp bands, characteristic of the Eu^{3+} ions emission, connected with the transitions from the excited $^5D_0$ level to ^7F_J (J = 1–4) levels. A small band at $\lambda = 536$ nm assigned to $^5D_1 \rightarrow {}^7F_1$ is also visible. Moreover, red emission band at 616 nm is much more intense comparing to the orange emission band at 594 nm. The emission color is redder instead of orange-red emission and the chromaticity of the core@shell nanomaterial is improved. This is consistent with the Eu^{3+} ion site symmetry, D_{2d}, with no inversion center. Intensity of the emission lines related to f–f transitions is dependent on the local site symmetry of the Eu^{3+} ions. Based on the selection rules, the magnetic dipole transitions are allowed and the electric dipole transitions are forbidden. When the Eu^{3+} ions occupy site with lack of inversion

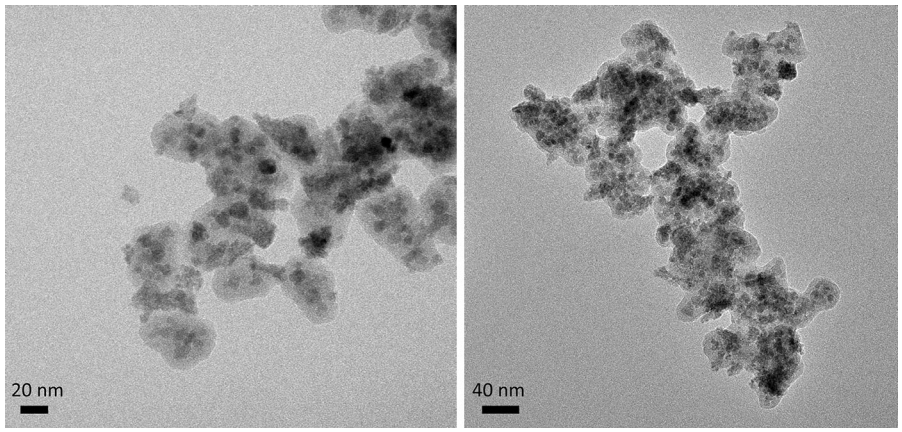

Fig. 4 TEM images of the synthesized Fe_3O_4@SiO_2@$GdVO_4$:Eu^{3+} 5 % core@shell nanostructures

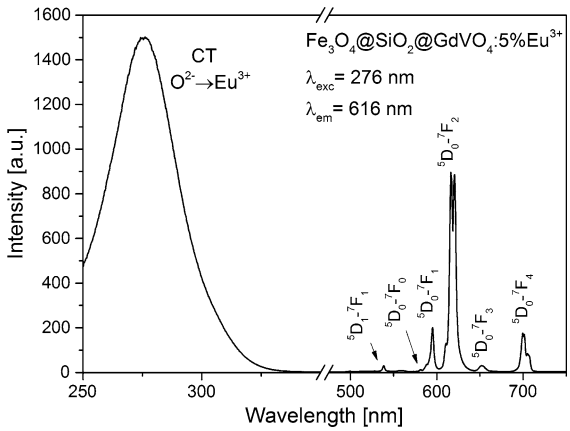

Fig. 5 Excitation (*left*) and emission (*right*) spectra of the Fe_3O_4@SiO_2@$GdVO_4$:Eu^{3+} 5 % core@shell-type nanostructure

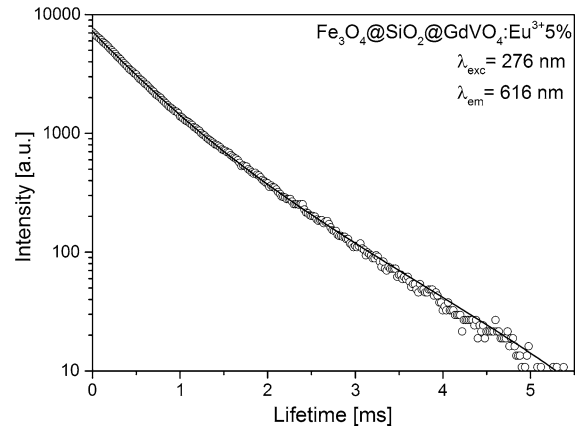

Fig. 6 Luminescence decay curves recorded for the Fe_3O_4@SiO_2@$GdVO_4$:Eu^{3+} 5 % core@shell-type nanostructure

symmetry, the intensities ratio of the $^5D_0$–$^7F_2$ to $^5D_0$–$^7F_1$ transitions should be relatively high, as in the case of Fe_3O_4@SiO_2@$GdVO_4$:Eu^{3+} 5 % core@shell-type nanostructure.

The recorded emission decay curve can be well fitted by a biexponential function and luminescent lifetimes were calculated and are equal to $\tau_1 = 0{,}49$ and $\tau_2 = 1{,}05$ ms, respectively (Fig. 6). The shorter component is connected with the Eu^{3+} ions located at the surface of crystallites, where the external environment strongly influences on the luminescent lifetime and quench the excited states.

In Fig. 7, luminescent and magnetic properties of the Fe_3O_4@SiO_2@$GdVO_4$:Eu^{3+} 5 % nanomaterial dispersed in water are presented. It is well seen that after magnet capture, all the nanoparticles were attracted to the magnet direction. Additionally, under UV light, the characteristic red luminescence of the Eu^{3+} ion was observed. The image showed confirms the formation of the bifunctional (magnetic–luminescent) Fe_3O_4@SiO_2@$GdVO_4$:Eu^{3+} 5 % core@shell-type nanomaterial.

The Fe_3O_4@SiO_2@$GdVO_4$:Eu^{3+} 5 % core@shell-type nanostructure did not influence the ESR (Fig. 8). Namely, the erythrocytes under nanoparticles treatment settled down with the same rate as the control cells.

The studied nanoparticles did not increase the erythrocyte membrane permeability and did not induce hemolysis up to concentration 1 mg/mL (results not shown). Moreover, nanoparticles treatment did not affect the discoid shape of erythrocytes

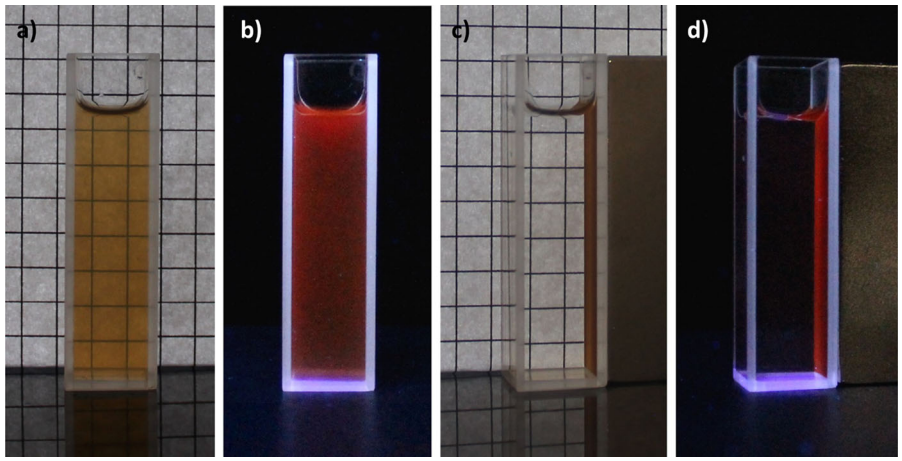

Fig. 7 Luminescent and magnetic properties of bifunctional Fe_3O_4@SiO_2@$GdVO_4$:Eu^{3+} 5 % core@shell-type nanostructure, before (**a**, **b**) and after (**c**, **d**) magnet capture. Presented sample was excited by UV lamp ($\lambda = 254$ nm)

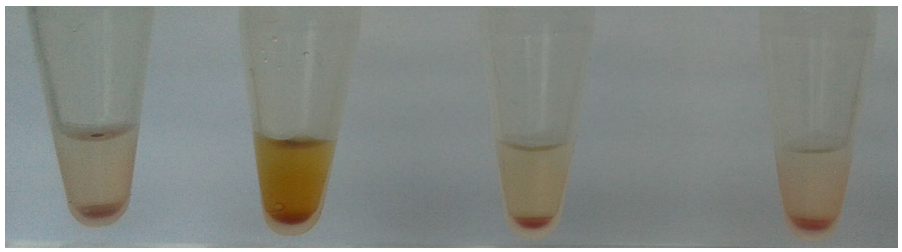

Fig. 8 The effect of the nanoparticles on the erythrocyte sedimentation rate. Nanoparticles concentration from the left: 0 mg/mL (control), 1, 0.1, 0.01 mg/mL

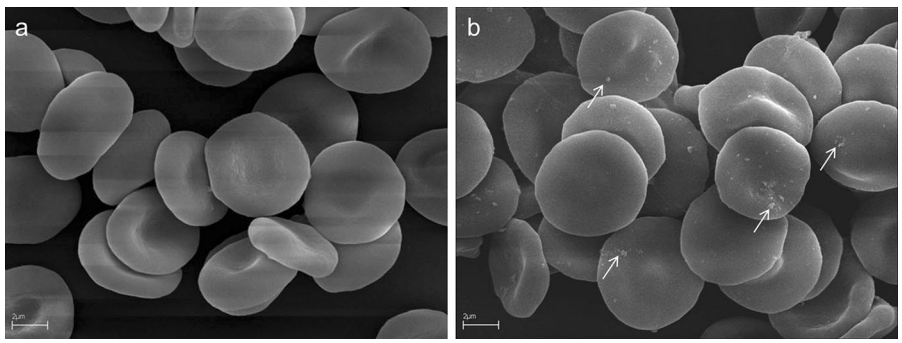

Fig. 9 The effect of Fe_3O_4@SiO_2@$GdVO_4$:Eu^{3+} 5 % core@-shell-type nanostructures, at the concentration 1 mg/mL on human erythrocytes morphology as observed by scanning electron microscope: **a** control cells, **b** cells incubated with core@shell nanostructures

(Fig. 9) although binding of nanoparticles to the erythrocyte membrane was detected (Fig. 9b). The white arrows indicate the core@shell-type nanostructures attached to the surface of erythrocytes.

Summing up, the studied nanostructures did not affect the ESR, neither morphology of red blood cells nor their membrane permeability. Therefore, we assume that the synthesized multifunctional nanomaterial

based on the doped rare earth orthovanadates is not toxic against human erythrocytes.

Conclusions

The luminescent-magnetic core@shell-type nanomaterial, Fe_3O_4@SiO_2@$GdVO_4$:Eu^{3+} 5 %, was successfully synthesized via a relatively simple and reproducible way. The obtained nanocomposite is composed of magnetic core, coated with a modified silica shell and surface decorated with red luminescent nanoparticles, having a long radiative lifetime. The nanocomposite synthesized has an average size about 40 nm and forms a stable aqueous colloid. When the magnetic field and UV light are applied the product reveals simultaneously bifunctional properties, namely intensive red luminescence and strong magnetism (the product follows by the applied magnet). What is more, the obtained luminescent-magnetic core@shell-type nanostructures do not exhibit toxicity against human erythrocytes, examined in vitro. All of the mentioned advantages of the nanomaterial synthesized allow its potential application in multimodal imaging, bio-labeling, drug delivery, targeted therapies, tracing techniques, forensics, and in other advanced applications.

Acknowledgments S.L., A. Sz., A.E.G, and T.G. kindly acknowledge the financial support from the National Science Centre (Grant DEC-2012/06/M/ST5/00325). M.R. gratefully acknowledges the financial support from the Polish Ministry of Science and Higher Education; scientific work was financed from the budget for science in 2012-2015 as a research project within the program called „Diamond Grant" Nr DI2011 011441. M.R. is a recipient of the scholarship from the Foundation of Adam Mickiewicz University in Poznań, for the 2014/2015 academic year. T.G. holds a scholarship from the Foundation for Polish Science for Young Scientists (FNP).

References

Bessis M, Weed RI, Leblond PF (1973) Red cell shape red cell shape; physiology, pathology, ultrastructure. Springer, Berlin, Heidelberg, pp 1–24. doi:10.1007/978-3-642-88062-9

Binnemans K (2009) Lanthanide-based luminescent hybrid materials. Chem Rev 109:4283–4374. doi:10.1021/cr8003983

Blasse G, Grabmaier BC (1994) Luminescent materials. Springer, Berlin

Chander H (2005) Development of nanophosphors—a review. Mater Sci Eng R Rep 49:113–155. doi:10.1016/j.mser.2005.06.001

Chen G, Desinan S, Nechache R, Rosei R, Rosei F, Ma D (2011) Bifunctional catalytic/magnetic Ni@Ru core-shell nanoparticles. Chem Comm 47:6308–6310. doi:10.1039/C1CC10619H

Cheng KH, Aijmo J, Ma L, Yao M, Zhang X, Como J, Hope-Weeks LJ, Huang J, Chen W (2008) Luminescence decay dynamics and trace biomaterials detection potential of surface-functionalized nanoparticles. J Phys Chem C 112:17931–17939. doi:10.1021/jp8065647

Cheng Z, Ma P, Hou Z, Wang W, Dai Y, Zhai X, Lin J (2012) YVO_4:Eu^{3+} functionalized porous silica submicrospheres as delivery carriers of doxorubicin. Dalton Trans 41:1481–1489. doi:10.1039/c1dt11399b

Corr SA, Rakovich YP, Gun'ko YK (2008) Multifunctional magnetic-fluorescent nanocomposites for biomedical applications. Nanoscale Res Lett 3:87–104. doi:10.1007/s11671-008-9122-8

Deshmukh AB, Devarapalli RR, Shelke MV (2014) Functional silicon nanostructures derived from drying-mediated self-assembly of gold nanoparticles. J Nanopart Res 16:2372. doi:10.1007/s11051-014-2372-8

Ding HL, Zhang YX, Wang S, Xu JM, Xu SC, Li GH (2012) Fe_3O_4@SiO_2 Core/Shell Nanoparticles: the silica coating regulations with a single core for different core sizes and shell thicknesses. Chem Mater 24:4572–4580. doi:10.1021/cm302828d

Dosev D, Nichkova M, Kennedy IM (2008) Inorganic lanthanide nanophosphors in biotechnology. J Nanosci Nanotechnol 8:1052–1067. doi:10.1166/jnn.2008.304

Gai S, Yang P, Li C, Wang W, Dai Y, Niu N, Lin J (2010) Synthesis of magnetic, up-conversion luminescent, and mesoporous core-shell-structured nanocomposites as drug carriers. Adv Funct Mater 20:1166–1172. doi:10.1002/adfm.200902274

Gnach A, Lipinski T, Bednarkiewicz A, Rybka J, Capobianco J (2014) Upconverting nanoparticles: assessing the toxicity. Soc. Rev, Chem. doi:10.1039/c4cs00177j

Grzyb T, Runowski M, Szczeszak A, Lis S (2012a) Influence of Matrix on the luminescent and structural properties of glycerine-capped, Tb^{3+}-doped fluoride nanocrystals. J Phys Chem C 116:17188–17196. doi:10.1021/jp3010579

Grzyb T, Szczeszak A, Rozowska J, Legendziewicz J, Lis S (2012b) Tunable luminescence of Sr_2CeO_4:M^{2+} (M = Ca, Mg, Ba, Zn) and Sr_2CeO_4:Ln^{3+} (Ln = Eu, Dy, Tm) nanophosphors. J Phys Chem C 116:3219–3226. doi:10.1021/jp208015z

Grzyb T, Runowski M, Dabrowska K, Giersig M, Lis S (2013) Structural, spectroscopic and cytotoxicity studies of TbF_3@CeF_3 and TbF_3@CeF_3@SiO_2 nanocrystals. J Nanopart Res 15:1958–1972. doi:10.1007/s11051-013-1958-x

Grzyb T, Runowski M, Lis S (2014) Facile synthesis, structural and spectroscopic properties of GdF_3:Ce^{3+}, Ln^{3+} (Ln^{3+}=Sm^{3+}, Eu^{3+}, Tb^{3+}, Dy^{3+}) nanocrystals with bright multicolor luminescence. J Lumin 154:479–486. doi:10.1016/j.jlumin.2014.05.020

Haidar ZS (2010) Bio-Inspired/-Functional colloidal core-shell polymeric-based nanosystems: technology promise in tissue engineering, bioimaging and nanomedicine. Polymers 2:323–352. doi:10.3390/polym2030323

Henglein A (1987) Q-particles: size quantization effects in colloidal semiconductors. Progr Colloid & Polymer Sci 73:1–4. doi:10.1007/3-798-50724-4_55

Holsa J (2009) Persistent luminescence beats the afterglow: 400 years of persistent luminescence. Electrochem Soc Interface Winter 18:42–45

Hu H, Wang Z, Pan L (2010) Synthesis of monodisperse Fe_3O_4@silica core–shell microspheres and their application for removal of heavy metal ions from water. J Alloys Compd 492:656–661. doi:10.1016/j.jallcom.2009.11.204

Huang S, Cheng Z, Ma P, Kang X, Dai Y, Lin J (2013) Luminescent $GdVO_4:Eu^{3+}$ functionalized mesoporous silica nanoparticles for magnetic resonance imaging and drug delivery. Dalton Trans 42:6523–6530. doi:10.1039/c3dt33114h

Jasiewicz B, Mrowczynska L, Malczewska-Jaskola K (2014) Synthesis and haemolytic activity of novel salts made of nicotine alkaloids and bile acids. Bioorg Med Chem Lett 24:1104–1107. doi:10.1016/j.bmcl.2014.01.005

Kang X, Yang D, Dai Y, Shang M, Cheng Z, Zhang X, Lian H, Ma P, Lin J (2013a) Poly(acrylic acid) modified lanthanide-doped $GdVO_4$ hollow spheres for up-conversion cell imaging, MRI and pH-dependent drug release. Nanoscale 5:253–261. doi:10.1039/c2nr33130f

Kang X, Yang D, Ma P, Dai Y, Shang M, Geng D, Cheng Z, Lin J (2013b) Fabrication of hollow and porous structured $GdVO_4:Dy^{3+}$ nanospheres as anticancer drug carrier and MRI contrast agent. Langmuir 29:1286–1294. doi:10.1021/la304551y

Li X, Yu M, Hou Z, Li G, Ma P, Wang W, Cheng Z, Lin J (2011) One-dimensional $GdVO_4:Ln^{3+}$ (Ln = Eu, Dy, Sm) nanofibers: Electrospinning preparation and luminescence properties. J Solid State Chem 184:141–148. doi:10.1016/j.jssc.2010.11.019

Limaye MV, Singh SB, Das R, Poddar P, Kulkarni SK (2011) Room temperature ferromagnetism in undoped and Fe doped ZnO nanorods: microwave-assisted synthesis. J Solid State Chem 184:391–400. doi:10.1016/j.jssc.2010.11.008

Liu J, Qiao SZ, Chen JS, Lou XW, Xing X, Lu GQ (2011) Yolk/shell nanoparticles: new platforms for nanoreactors, drug delivery and lithium-ion batteries. Chem. Comm. 47:12578–12591. doi:10.1039/c1cc13658e

Lou L, Yu K, Zhang Z, Li B, Zhu J, Wang Y, Huang R, Zhu Z (2011) Functionalized magnetic-fluorescent hybrid nanoparticles for cell labelling. Nanoscale 3:2315–2323. doi:10.1039/c1nr10066a

Lu P, Zhang J-L, Liu Y-L, Sun D-H, Liu G-X, Hong G-Y, Ni J-Z (2010) Synthesis and characteristic of the Fe_3O_4@-SiO_2@$Eu(DBM)_3.2H_2O/SiO_2$ luminomagnetic microspheres with core-shell structure. Talanta 82:450–457. doi:10.1016/j.talanta.2010.04.052

Ma Q, Wang J, Dong X, Yu W, Liu G (2014) Electrospinning fabrication and characterization of magnetic-upconversion fluorescent bifunctional core–shell nanofibers. J Nanopart Res 16:2239. doi:10.1007/s11051-013-2239-4

Massart R (1981) Preparation of aqueous magnetic liquids in alkaline and acidic media. IEEE Trans Magn 17:1247–1248. doi:10.1109/TMAG.1981.1061188

Niu N, Yang P, Liu Y, Li C, Wang D, Gai S, He F (2011) Controllable synthesis and up-conversion properties of tetragonal $BaYF_5$:Yb/Ln (Ln = Er, Tm, and Ho) nanocrystals. J Colloid Interface Sci 362:389–396. doi:10.1016/j.jcis.2011.07.001

Nuñez NO, Rivera S, Alcantara D, de la Fuente JM, García-Sevillano J, Ocaña M (2013) Surface modified Eu:$GdVO_4$ nanocrystals for optical and MRI imaging. Dalton Trans 42:10725–10734. doi:10.1039/c3dt50676b

Park J-N, Zhang P, Hu Y-S, McFarland EW (2010) Synthesis and characterization of sintering-resistant silica-encapsulated Fe_3O_4 magnetic nanoparticles active for oxidation and chemical looping combustion. Nanotechnology 21:225708–225716. doi:10.1088/0957-4484/21/22/225708

Runowski M, Grzyb T, Lis S (2011) Bifunctional luminescent and magnetic core/shell type nanostructures Fe_3O_4@-$CeF_3:Tb^{3+}/SiO_2$. J Rare Earths 29:1117–1122. doi:10.1016/S1002-0721(10)60609-6

Runowski M, Grzyb T, Lis S (2012) Magnetic and luminescent hybrid nanomaterial based on Fe_3O_4 nanocrystals and $GdPO_4:Eu^{3+}$ nanoneedles. J Nanopart Res 14:1188–1195. doi:10.1007/s11051-012-1188-7

Runowski M, Dabrowska K, Grzyb T, Miernikiewicz P, Lis S (2013) Core/shell-type nanorods of Tb^{3+}-doped $LaPO_4$, modified with amine groups, revealing reduced cytotoxicity. J Nanopart Res 15:2068–2083. doi:10.1007/s11051-013-2068-5

Runowski M, Ekner-Grzyb A, Mroczynska L, Balabhadra S, Grzyb T, Paczesny J, Zep A, Lis S (2014) Synthesis and organic surface modification of luminescent, lanthanide-doped core/shell nanomaterials (LnF_3@SiO_2@NH_2@Organic Acid) for potential bioapplications: spectroscopic, structural, and in vitro cytotoxicity evaluation. Langmuir 30:9533–9543. doi:10.1021/la501107a

Selvan ST, Tan TTY, Yi DK, Jana NR (2009) Functional and multifunctional nanoparticles for bioimaging and biosensing. Langmuir 26:11631–11641. doi:10.1021/la903512m

Shanta Singh N, Kulkarni H, Pradhan L, Bahadur D (2013) A multifunctional biphasic suspension of mesoporous silica encapsulated with $YVO_4:Eu^{3+}$ and Fe_3O_4 nanoparticles: synergistic effect towards cancer therapy and imaging. Nanotechnology 24:065101. doi:10.1088/0957-4484/24/6/065101

Tong L, Shi J, Ren X, Li Q, Ding H, Yang H (2013) Multifunctional nanocomposites with different coupling agents: synthesis, luminescent and magnetic properties. J Nanopart Res 15:1627. doi:10.1007/s11051-013-1627-0

Wang Y, Qin W, Zhang J, Cao C, LU S, Ren X (2009) Photoluminescence of colloidal YVO_4:Eu/SiO_2 core/shell nanocrystals. Opt Commun 282:1148–1153. doi:10.1016/j.optcom.2008.12.007

Wang C, Yin D, Ouyang J, Song K, Liu B, Wu M (2014) Synthesis of fluorescent and magnetic bi-functional $NaLuF_4$-based upconversion nanocrystals. J Nanosci Nanotechnol 14:5232–5237. doi:10.1166/jnn.2014.8672

Wu J, Yan B (2008) Photoluminescence intensity of $YxGd_{1-x}VO_4:Eu^{3+}$ dependence on hydrothermal synthesis time and variable ratio of Y/Gd. J Alloys Compd 455:485–488. doi:10.1016/j.jallcom.2007.01.162

Xue X, Wang F, Liu X (2011) Emerging functional nanomaterials for therapeutics. J Mater Chem 21:13107–13127. doi:10.1039/c1jm11401h

Yang D, Kang X, Shang M, Li G, Peng C, Li C, Lin J (2011) Size and shape controllable synthesis and luminescent properties of $BaGdF_5:Ce^{3+}/Ln^{3+}$ (Ln = Sm, Dy, Eu, Tb) nano/submicrocrystals by a facile hydrothermal process. Nanoscale 3:2589–2595. doi:10.1039/c1nr10203f

Yin W, Zhou L, Gu Z, Tian G, Jin S, Yan L, Liu X, Xing G, Ren W, Liu F, Pan Z, Zhao Y (2012) Lanthanide-doped $GdVO_4$ upconversion nanophosphors with tunable emissions and their applications for biomedical imaging. J Mater Chem 22:6974–6981. doi:10.1039/c2jm16152d

Yoo J-H, Lee S-W (2014) Fabrication and characterization of quantum dots-bound hydrogels with fluorescent and temperature-sensitive functionalities. J Nanosci Nanotechnol 14:7648–7653. doi:10.1166/jnn.2014.9411

Zhou J, Lu Z, Shan G, Wang S, Liao Y (2014) Gadolinium complex and phosphorescent probe-modified $NaDyF_4$ nanorods for T1- and T2-weighted MRI/CT/phosphorescence multimodality imaging. Biomaterials 35:368–377. doi:10.1016/j.biomaterials.2013.09.088